

ISABE-2011-1122

CFD INVESTIGATION OF SWIRL-STABILIZED FLEXI-FUEL BURNER USING METHANE-AIR MIXTURE FOR GAS TURBINES

Abdallah Abou-Taouk

Chalmers University of Technology
Applied Mechanics
Gothenburg, 41296 Sweden

Ronald Whiddon

Lund University
Department of Combustion Physics
Lund, Sweden

Ivan R. Sigfrid

Lund University
Department of Energy
Sciences
Lund, Sweden

Lars-Erik Eriksson

Chalmers University of
Technology
Applied Mechanics
Gothenburg, 41296 Sweden

Abstract

Combustion modeling based on a multi-step global reaction mechanism [1] is applied to CFD (Computational Fluid Dynamics) analysis of a scaled swirl-stabilized 4th generation premixed DLE (Dry Low Emission) burner for gas turbines. The flexi-fuel burner consists of a MAIN premixed flame, a premixed PILOT flame and a confined RPL (Rich Pilot Lean) flame. Both steady-state RANS (Reynolds Averaged Navier Stokes) and hybrid URANS/LES (Unsteady RANS/Large Eddy Simulation) results have been computed. The results are compared with high quality experimental data in the form of emission data, PIV (Particle Image Velocimetry) data and OH-PLIF (Planar Laser Induced Fluorescence Imaging) from an atmospheric burner test rig at Lund University [2-3]. There is a good agreement between the CFD simulations and measurements of emissions, velocity field and flame visualization.

Nomenclature

CFD	Computational Fluid Dynamics
CH ₄	Methane gas
CO	Carbon monoxide
CO ₂	Carbon dioxide

DLE	Dry Low Emission
EDM	Eddy Dissipation Model
FRC	Finite Rate Chemistry
LCV	Low Caloric Value
LES	Large Eddy Simulation
MFC	Mass Flow Controllers
PIV	Particle Image Velocimetry
PLIF	Planar Laser-Induced Fluorescence Imaging
PSR	Perfectly Stirred Reactor
RANS	Reynolds Averaged Navier Stokes
RPL	Rich Pilot Lean
SCADA	Supervisory Control and Data Acquisition
SAS	Scale Adaptive Simulation
SIT	Siemens Industrial Turbomachinery
SST	Shear Stress Transport
URANS	Unsteady Reynolds Averaged Navier Stokes

Introduction

Combustion of fossil fuels will remain the dominating energy conversion process for at least the next 50 years [4]. Improved combustion technology in terms of efficiency and pollutant emissions is therefore crucial. During the last few years the development of combustor technology has followed a general trend towards fuel-flexibility and increased use of bio fuels. This comes from the

increased pressure to reduce carbon dioxide emissions from fossil fuels.

The premixed scaled 4th generation DLE burner is supplied by SIT (Siemens Industrial Turbomachinery), which was developed, in part, to be fuel flexible. The high swirl flow in the SIT burner is extremely challenging from an aerodynamic and combustion point of view, especially since this combustor is comprised of a lean premixed MAIN part, a premixed PILOT and a RPL radical pool generator. These systems together create a complex geometry with many details included. Reliable and robust design of combustors depends on a good understanding of the chemical and physical properties of fuels. Prediction of combustor performance, including efficiency, ignition, flame stability and emissions characteristics, requires both detailed modeling and advanced measuring techniques.

The chemistry of methane-air combustion is here chosen for the simulations since methane as a fuel is included in the experimental part. Although methane-air combustion is considerably simpler than that of higher hydrocarbons, a detailed mechanism still involves many elementary reactions and species. For this type of complex reaction scheme the computational time will be too large. To save computational time the number of reactants and species has to be limited to a few global reactions. Several different reduced reaction mechanisms of methane-air mixture exist in the literature [5-11].

In this work, a 3-step optimized global reaction mechanism for methane-air mixture is applied and validated in subsequent CFD analysis. The 3-step optimized global reaction mechanism contains correction functions that depend on the equivalence ratio [1]. This mechanism is optimized against a

detailed reference mechanism (GRI Mech 3.0 [12]) for PSR (Perfectly Stirred Reactor) calculations. The CANTERA software [13] has been used for the detailed mechanism simulations and an in-house PSR code was used for the global reaction mechanism.

In swirl-stabilized flames the interactions between chemistry and turbulence is complex. The coupling between turbulence and combustion is modeled in the CFD code (Ansys CFX [15]) by the combined EDM (Eddy Dissipation Model) [16] and Finite Chemistry Model (FCM).

The grid generation of the scaled 4th generation DLE flexi-fuel burner required a lot of effort since only structured hexahedral (hex)-cells were used. The hex mesh is preferred over tetrahedral-mesh since the hex-cells gives lower numerical dissipation (the mesh cells are in line with the general flow direction) and lower cell count (a factor of 8 lower). It is extremely important to keep the cell count down since it is directly proportional to the simulation time needed for a converged solution.

In support and verification of the CFD simulations, measurements were taken for various aspects of burner function. These measurements include emissions values at many burner operation points, including onset of lean blowout, and PIV in the combustor. Though not directly tracked in CFD, OH radical PLIF images have been recorded at the same operating point as the PIV measurements.

The aim of the CFD investigation is to improve, validate and evaluate current industrial CFD tools and modeling procedures for a new type of flexi-fuel combustors, the scaled 4th generation DLE flexi-fuel burner, developed at SIT.

Experiment

All experiments have been carried out using a scaled 4th generation DLE flexi-fuel burner designed by SIT.

A. System description

The burner is composed of three concentric sectors each with discrete equivalence ratio control. The burner can be coupled to either a square or cylindrical combustion liner, which terminates in a conical contraction before dumping to exhaust. The square combustion liner is composed of a quartz lower portion and steel upper section with respective lengths of 260mm and 400mm, and cross section of 105cm². Additionally, a 700mm steel cylindrical combustion liner was used during emission measurements with a cross section of 53cm².

The three concentric regions from center to outermost are designated the MAIN, PILOT and RPL sectors. Fuel to each of the three sectors is individually controlled by respective Alicat Scientific MFC (Mass Flow Controllers). The air flow to the RPL is also controlled by an Alicat MFC, allowing independent control of the RPL sector. Air to the PILOT and MAIN sectors is supplied by two Rieschle SAP 300 blowers, which are controlled by a variable frequency AC driver. Flow meters at the blower outlet monitor air flow to the PILOT and MAIN sectors of the burner, whose design distributes 21% of the air to the PILOT and 79% to the MAIN sector. Blower control, flow monitoring and MFC's are all coupled to an in-house LabView control program.

The total fuel and air flow during the measurements were 75 g/s. The flow through the RPL was 1.5 g/s. The RPL equivalence ratio was 1.2. The MAIN and PILOT equivalence ratios were set to the same value, equivalence ratio 0.39. The total equivalence ratio was 0.41, which corresponds to an adiabatic flame

temperature of 1600K. The inlet air temperature was set to 650K and the fuel was at room temperature (298K).

B. Measurement setup

Emissions measurements were made using the cylindrical steel combustion liner. An emission probe, located 75mm from the exit of the liner contraction (see Figure 1) sampled, simultaneously, several points across the exit flow to obtain an average value. The CO measurements cited in this work were made with a Rosemount Analytical Binos-100 CO/CO₂ gas analyzer, and are an average of 30 measurements taken for each equivalence ratio tested.

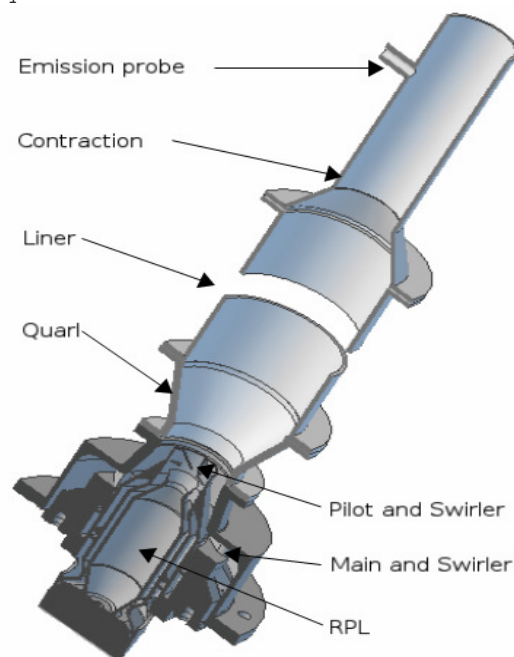


Figure 1. Three sector experimental DLE burner, cylindrical liner shown as used in emissions measurements

Optical measurements were made using the quartz and steel combustion liner and also without the liner present. A schematic of the confined type measurement setup is shown in Figure 1 and Figure 2.

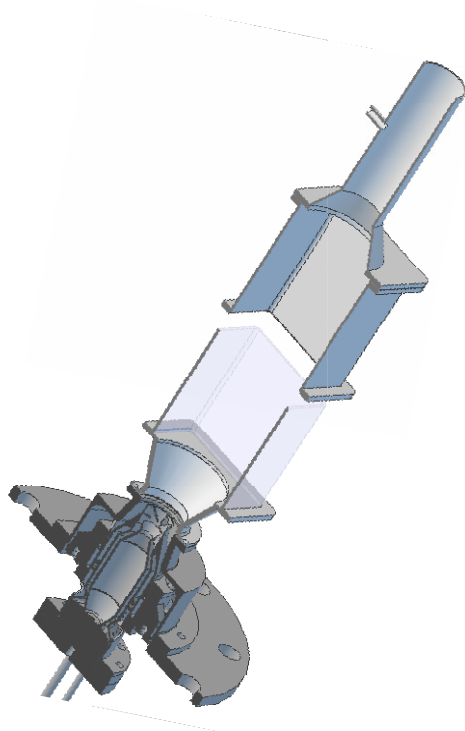


Figure 2. Experimental burner with a square liner used for the PIV measurements

The PIV system is sourced from LaVision, and features a pair of Brilliant-B Nd:YAG lasers, overlapped in a "Twins" frequency doubling unit. The beam then passed through a diverging sheet-optics lens pack before passing through the square cross-section, quartz combustion liner. The laser sheet was focused outside of the combustion liner, resulting in a sheet thickness of approximately 3mm; the sheet height was approximately 130mm upon entrance to the liner. The camera used was a LaVision Imager Intense frame transfer camera with resolution of 1376x1040 pixels. The experimental setup can be seen in Figure 3. As well as PIV measurements, OH-PLIF measurements were taken. A Nd:YAG laser was used to pump a dye laser which, with doubling, was used to excite fluorescence from the OH radical, a combustion intermediate. The laser sheet is formed in the same plane as the PIV measurements; however, custom sheet optics was

used, resulting in a significantly smaller sheet than was used for PIV.

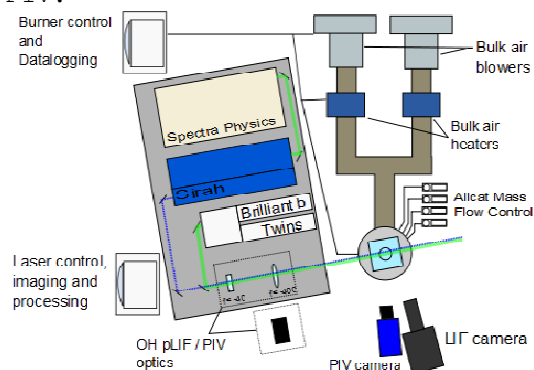


Figure 3. Experimental setup/ Lasers/ Optics and camera. PIV and OH-PLIF lasers are coincident in their path through the burner, though optics were changed depending on measurement

Laser, camera control and PIV vector processing were all handled by the DaVis 7.2.2 software package. PIV settings are summarized in Table 1. PIV vector fields from confined and unconfined conditions are shown in Figure 4 and Figure 5 respectively. For the confined case, vector measurements could not be made at the edge of the confinement due to reflections at the front and rear windows. Notably is the reflections from the rear window. These reflections, specially close to the quarl, influence the PIV measurements giving cause to bad vectors. This can clearly be seen in Figure 17, axial positions 0-60mm.

Table 1 PIV parameters

Interrogation window	32x32 pixels
Pixel size	118 um
Image processing	Crosscorrelation 50% overlap
Optical window	~120 x ~160 mm
Laser power	~100 mJ/pulse
Camera CCD	1376x1040 pixels
Seeding particles	Aerosil-200
Optical filter	532 nm interference
Camera lens	Nikkor 60 mm
Pulse separation	15 us

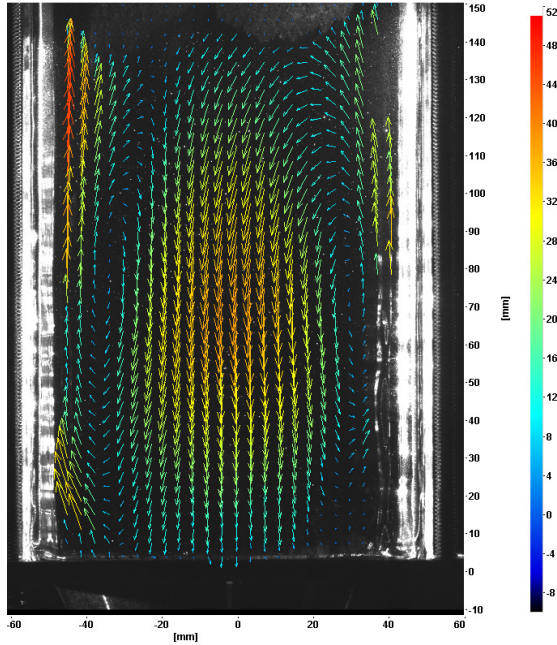


Figure 4. Post processed PIV velocity field with the square quartz liner

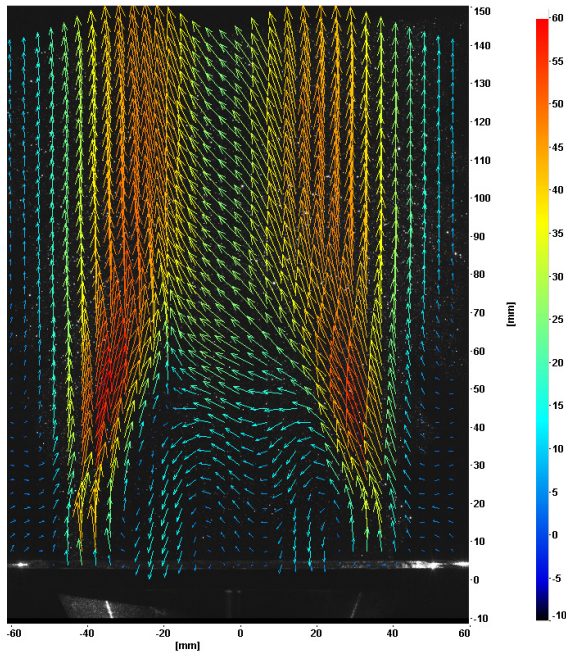


Figure 5. Post processed PIV velocity field without liner

Kinetic Modeling

The optimized 3-step global reaction mechanism consists of the reactions seen in Table 2. The first reaction is the oxidation of methane into CO and H₂O and the second reaction is the oxidation of CO into CO₂. Table 2 also shows the optimized Arrhenius coefficients (activation energy, pre-exponential factor and temperature coefficient) that are used in the 3-step global reaction mechanism.

Reaction	A	E _a [J/kmol]	β
2CH ₄ +3O ₂ →2CO+4H ₂ O	1.398762e10	1.16712e8	-0.062
2CO+O ₂ ↔2CO ₂	7.381123e11	7.65969e7	0.215

Table 2. Activation energy E_a, pre-exponential factor A and temperature coefficient β used for the optimized scheme

The backward rate for the second reaction is based on an equilibrium assumption and the reaction rates for the forward reactions are the following:

$$RR_1 = f_1(\phi)T^{\beta_1}A_1e^{-\frac{E_{a1}}{RT}}[CH_4]^{0.5}[O_2]^{1.066} \quad 1.$$

$$RR_2 = f_2(\phi)T^{\beta_2}A_2e^{-\frac{E_{a2}}{RT}}[CO]^2[O_2]^1 \quad 2.$$

where A is the pre-exponential factor, E_a is the activation energy, R is the gas constant, T is the temperature and f₁ and f₂ are the correction functions. The aim of these correction functions is to ensure good agreement for rich conditions. Franzelli et al. [14] optimized similar correction functions, but for kerosene fuel and therefore one expects to see some differences in the shape of these functions for methane air-mixture, which can be seen in Figure 6. In a comparison of the optimized 3-step global reaction mechanism with the reference detailed reaction mechanism, GRI Mech 3.0, the results show that the gas temperature and emissions are reasonably well predicted for lean and rich conditions [1]. Figure 7 shows the temperature predictions at different equivalence ratios.

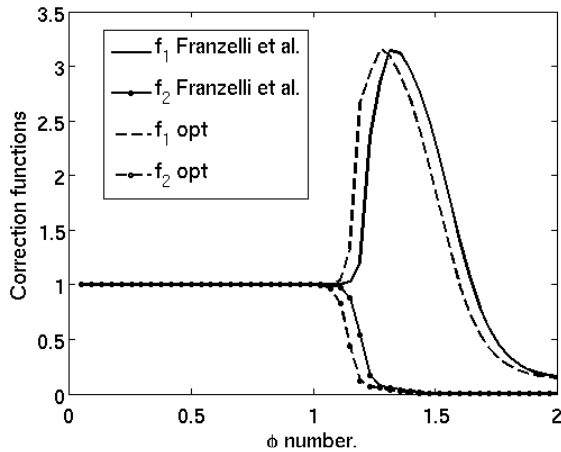


Figure 6. Plot showing the correction functions f_1 and f_2 between Franzelli et al. [14] (for kerosene fuel) and Abou-Taouk et al. [1] (methane-air mixture)

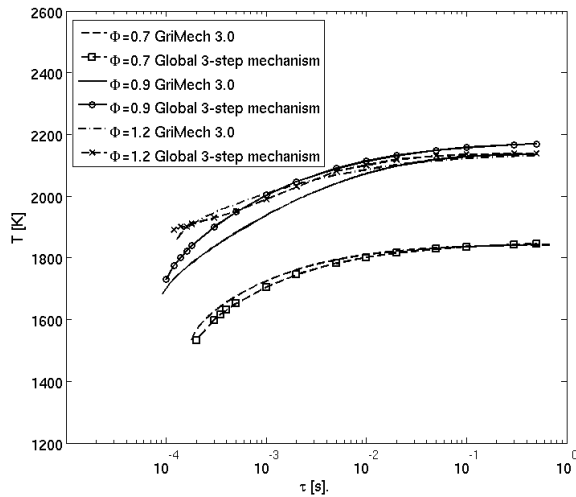


Figure 7. Plot showing temperature comparisons of a detailed mechanism (Gri Mech 3.0) and optimized 3-step global mechanism for methane-air gas mixture at equivalence ratios of 0.7, 0.9 and 1.2, $T_{in}=295K$

TURBULENCE-Chemistry interaction

The combined turbulence-chemistry interaction model, the Finite Rate Chemistry/Eddy Dissipation Model, in Ansys CFX [14-15], was chosen for all CFD analyses. The FRC model computes the reaction rates R_1 and R_2 by the following expressions:

$$R_1 = f_1(\phi)F_1[CH_4]^{0.5}[O_2]^{1.066} \quad 3.$$

$$R_2 = f_2(\phi)F_2[CO]^2[O_2]^1 - B_2[CO_2]^2 \quad 4.$$

where the forward and backward rate constants assume the following expressions:

$$F_1 = A_1 T^{\beta_1} e^{-\frac{E_{a1}}{RT}} \quad 5.$$

$$F_2 = A_2 T^{\beta_2} e^{-\frac{E_{a2}}{RT}} \quad 6.$$

$$B_2 = \frac{F_2}{K_C} \quad 7.$$

where A_k is pre-exponential factor, β_k is the temperature exponent, E_k is the activation energy and K_C the equilibrium constant. The FRC model computes one reaction rate respectively for each reaction in the optimized global reaction mechanism.

In the EDM model, the reaction rate of reaction k , is computed as:

$$R_k = A \frac{\varepsilon}{k} \min\left(\frac{[I]}{v'_{kl}}\right) \quad 8.$$

where A is a constant, $\frac{\varepsilon}{k}$ is the turbulent mixing rate, $[I]$ is the molar concentration of component I and v'_{kl} represent the reaction order of component I in the reaction k . The EDM model computes one reaction rate respectively for each reaction in the optimized global reaction mechanism. The EDM model is based on the work of Magnussen and Hjertager [16].

The combined FRC-EDM model thus gives two different reaction rates for each reaction, one from the EDM model and one from the FRC model. The minimum rate for each reaction is then chosen.

CFD modeling

Both steady-state RANS and time-averaged hybrid unsteady RANS/LES simulations were performed to predict flow and combustion dynamics. Three different models were investigated, one with circular liner (Figure 8), one with a square liner (Figure 9) and one with an "open" liner (unconfined flame, Figure 10).

Computational model and boundary conditions

The numerical prediction of the complex 3D swirling flow and the combustion process is computationally expensive and therefore is the boundary layer unresolved. Three different computational models are modeled in this paper, see Figure 8 - Figure 10. The circular liner has been used for comparisons with the emission data. The other two have been used for comparison with PIV measurements and OH-PLIF images. The simulations were performed on a 360° model since there is no periodic condition in the models.



Figure 8. Computational domain with a circular liner

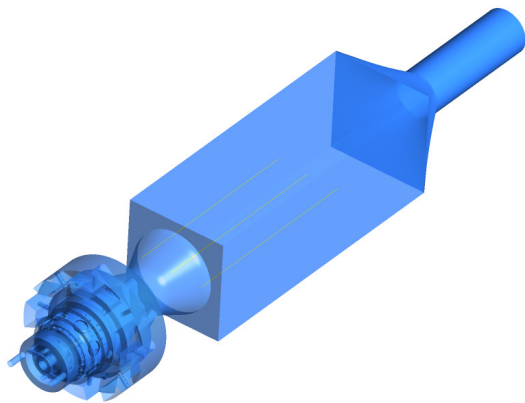


Figure 9. Computational domain with a square liner

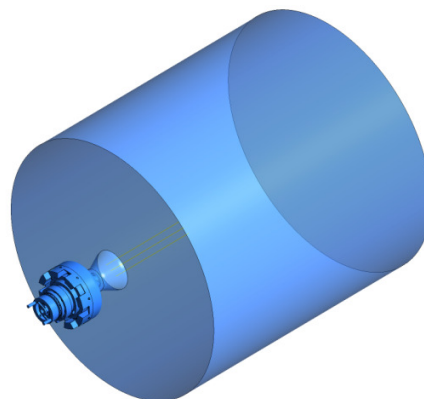


Figure 10. Computational domain with an "open liner" (unconfined flame)

The CFD simulations contain all the complex 3D geometry from the experimental set-up, i.e. guide vanes for MAIN and RPL systems, air and fuel cavities, cooling holes and ribs, etc.

The specified mass flow is used as the boundary condition for the six inlets, see Figure 11. The total temperature for the fuel and RPL air is set to 300K. The MAIN and PILOT air systems are preheated to 650K. The outlet boundary condition is set to atmospheric pressure, and all the walls are set to no-slip adiabatic walls. The geometry with the open liner features a co-flow surrounding the burner.

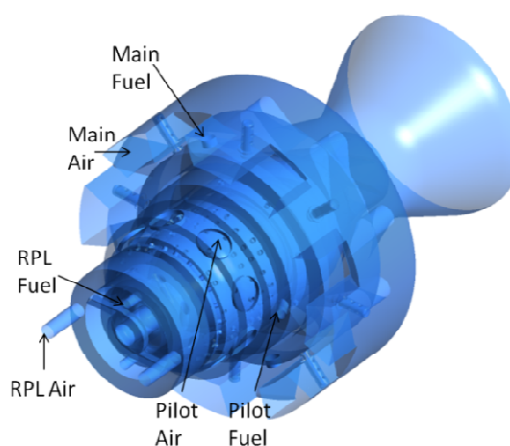


Figure 11. Configuration of the combustor inlets

A. Numerical method

The Ansys CFX commercial software package [15] was used to perform the CFD simulations. The $k\omega$ -SST 2-equation turbulence model (Shear Stress Transport model) [17] was selected for the steady-state simulations.

The SAS-SST (Scale Adaptive Simulation) turbulence model is used for the transient simulations. The model is based on the introduction of the von Karman length scale into the turbulence scale equation. The information provided by the von Karman length scale allows the SAS model to adjust in order to resolve structures in a URANS simulation, which results in LES-like behavior in unsteady regions of the flow field. At the same time, the model provides standard RANS behavior in regions of stable flow [18].

The benefits with the SAS-SST model compared to the LES simulation is the higher time step that one can use. The courant number can be up to 10 in the SAS-SST model, while in the LES the courant number needs to be below 1. Also, the SAS-SST model does not need as high a mesh resolution as the LES simulation.

B. Computational mesh

A grid independence study has been done for the burner [1]. The chosen fine mesh is a multi-block structured mesh containing approximately 10 million hexahedral cells. Figure 12 shows the structured grid of the scaled swirl-stabilized 4th generation premixed DLE burner. The ICEM CFD commercial software [19] has been used for the meshing.

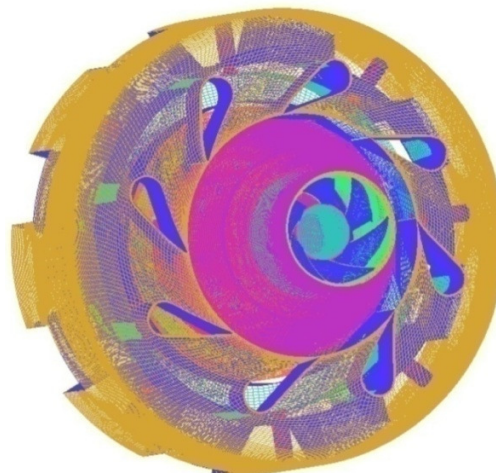


Figure 12. Structured hexahedral mesh, aft view

C. Convergence

Conservation checks were made for mass, momentum, energy and major species (CO_2 , CO , CH_4). The mass was within $\pm 0.1\%$, energy within $\pm 0.4\%$, momentum within $\pm 0.04\%$ and major species within $\pm 2\%$. Ten monitor points were also positioned at different locations in the burner to check that convergence had been obtained in the burner with respect to temperature, pressure and species concentrations.

Results and discussion

This section is divided in two parts, emission data and flow field.

A. Emission data

The geometry used here for comparisons is the cylindrical liner, see Figure 8. The data is published by Sigfrid et al. [1-2].

Figure 13 and Figure 14 show CO and O_2 mass fractions extracted from the averaged transient CFD (SAS-SST) compared to the experimental data close to the MAIN exit. Different values of the RPL equivalence ratios (0.8-1.6) have been used in the experiment. The equivalence ratio for the MAIN and PILOT systems is equal and adjusted to have the total equivalence ratio shown in Figure 13 and Figure 14.

The agreement between the experimental data and the 3-step global reaction mechanism is very good. The optimized mechanism gives a good prediction of the CO at rich conditions in the RPL. For equivalence ratio equal to 0.8 in the RPL, the lean blow out limit defined by an increase in CO emissions was not reached. The reason for this is due to combustion instabilities caused the flame to extinguish before the limit could be reached.

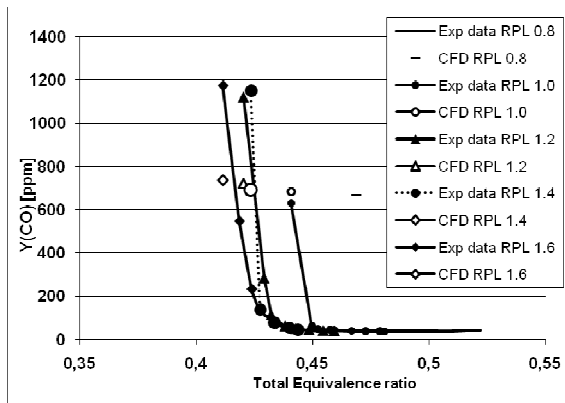


Figure 13. CO mass fraction plotted at different equivalence ratios for the RPL compared to the experimental data

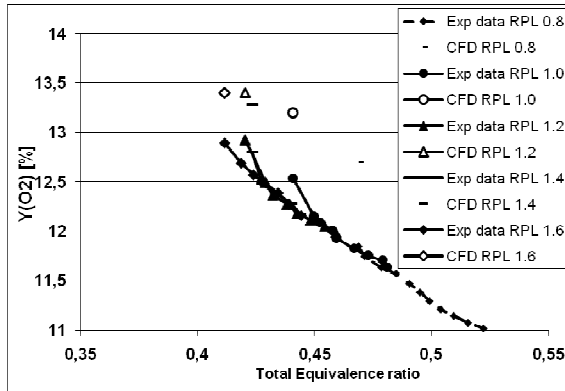


Figure 14. O₂ mass fraction plotted at different equivalence ratios for the RPL compared to the experimental data

B. Flow field

The equivalence ratio for the experimental point is set to 1.2 in the RPL system and to 0.39 in the MAIN and PILOT systems. The total equivalence ratio is 0.41 in the burner. The same settings have been used for the quadratic and open liner.

i. Quadratic liner

Figure 16 - Figure 18 show results from the steady-state RANS and the transient SAS-SST simulation at three different axial lines, see Figure 15, compared to the PIV measurements.

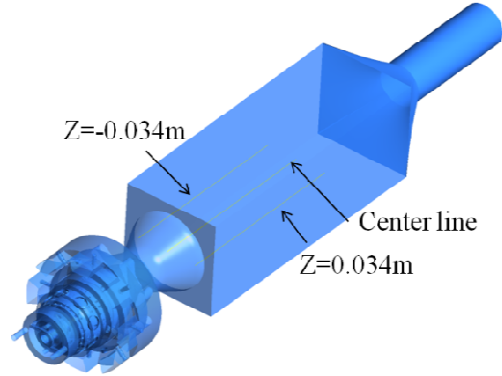


Figure 15. Different axial lines located at different Z coordinates

RANS fails in prediction of the size of the recirculation zone at $Z=-0.034\text{m}$ and at center line. The SAS-SST model predicts the recirculation zone at these two positions well and the position and magnitude of the highest velocity quite well. At $Z=0.034\text{m}$ both RANS and SAS-SST models predicts poorly the upstream axial velocity. The explanation of this can be due to the measurements are strongly affected by reflections in axial position 0-0.06m. The RANS model underpredicts the highest absolute axial velocity at all locations.

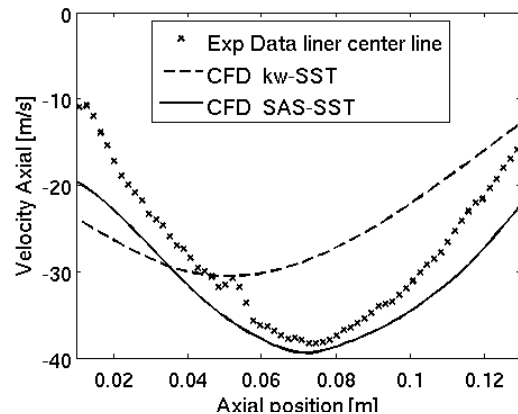


Figure 16. Axial velocity [m/s] computed at the center line for steady state and transient CFD-simulations compared to the experimental data

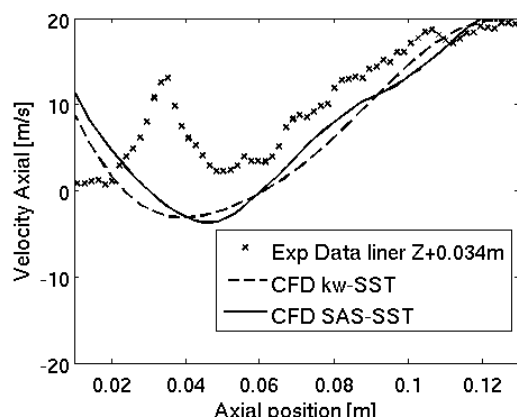


Figure 17. Axial velocity [m/s] computed on a line located at $Z=0.034\text{m}$ for steady state and transient CFD-simulations compared to the experimental data, the measurements are strongly affected by reflections in axial position 0-0.06m

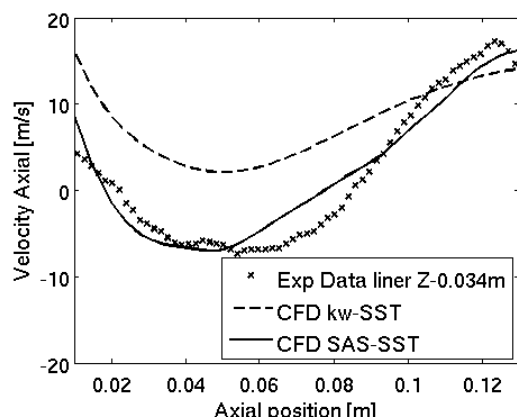


Figure 18. Axial velocity [m/s] computed on a line located at $Z=-0.034\text{m}$ for steady state and transient CFD-simulations compared to the experimental data

Figure 19 and Figure 20 show mean velocity vector field from the PIV measurements and transient averaged CFD. The CFD over-predicts slightly the size of the recirculation zone. In general, the CFD captures the locations of the recirculation zones well.

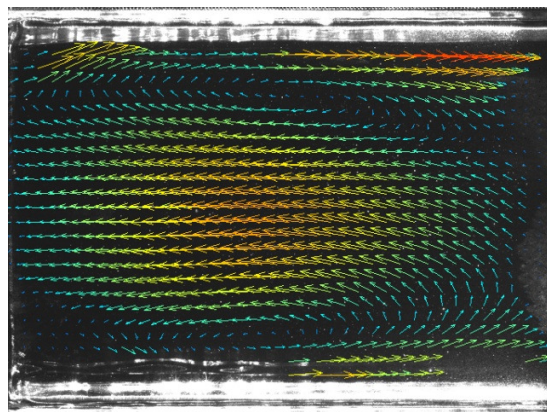


Figure 19. Velocity vector field from the experimental measurements, where the range is from 0m/s (blue color) to 52m/s (red color)

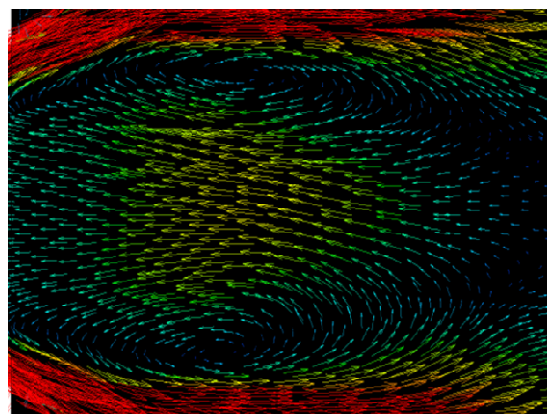


Figure 20. Velocity vector field from averaged transient CFD simulation, where the range is from 0m/s (blue color) to 52m/s (red color)

Figure 21 below shows the reaction rate for the methane oxidation (first reaction) using the SAS-SST model. The data in the plot are transient averaged. The highest reaction rate is located in the divergent cylinder. Also, high reaction rate is located upstream in the square liner, close to the walls. This is in good agreement with the results from the OH-PLIF, shown in Figure 22 and Figure 23.

Figure 22 shows six different instantaneous plots of the OH radical and Figure 23 shows the averaged plot of OH radical. The flow direction is from the bottom

of the plots and directed upwards in the figures. The highest amount of OH-radicals is located near the region where the reaction rate for the methane oxidation is highest in the CFD-simulation (Figure 21).

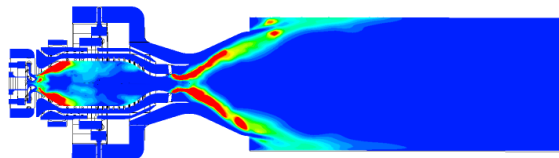


Figure 21. Averaged transient reaction rate for methane oxidation using the SAS-SST model. Red means the highest reaction rate and blue the lowest reaction rate

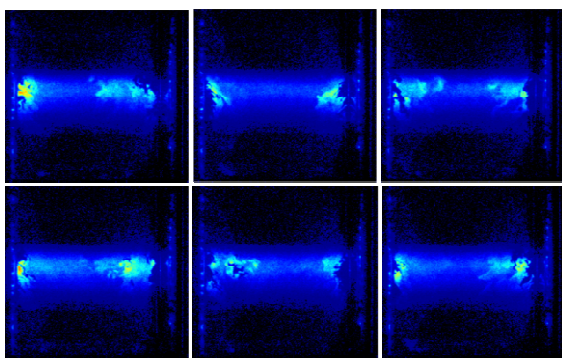


Figure 22. Instantaneous plots from OH-PLIF measurements showing the OH radical at six different times, the quarl (see Figure 2) is located in the bottom of the figures

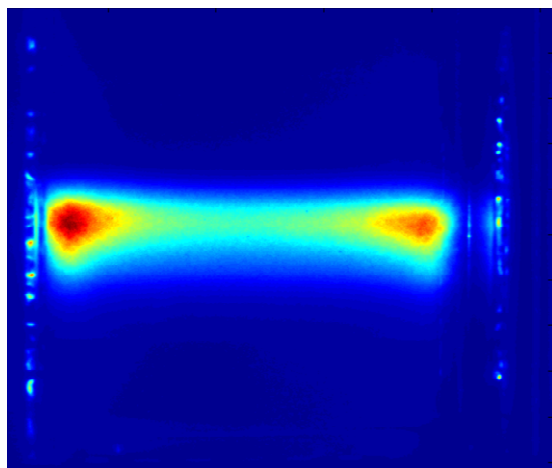


Figure 23. Averaged plot from the OH-PLIF measurements showing the OH radical, the quarl (see Figure 2) is located in the bottom of the figure

ii. Open liner (unconfined flame)

Figure 24 - Figure 26 show results from the steady-state RANS and the SAS-SST simulation at three different axial lines located at different z-coordinates compared to the PIV measurements. The reason to chose axial lines at position $Z=+15\text{mm}$ at the unconfined flame and $Z=+34\text{mm}$ at the confined flame is due to the smaller recirculation zone in the unconfined flame. The flame and recirculation zone is around three times smaller than the case with square liner. The RANS simulation seems to predict the axial velocity downstream better than the SAS-SST model. One reason for this may be that in the CFD a co-flow is introduced around the burner to model the experiment setup without a liner. This co-flow may influence the flame downstream in the burner. Also, in the experimental setup a fan is located above the burner to extract the exhaust gases. This fan is not included in the CFD and may affect the recirculation zones in the experiment.

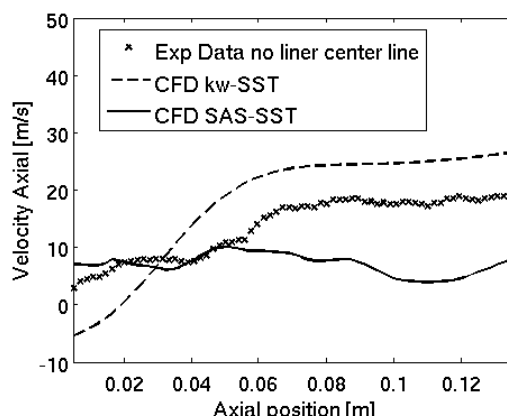


Figure 24. Axial velocity [m/s] computed at the center line for steady state and transient CFD-simulations compared to the experimental data

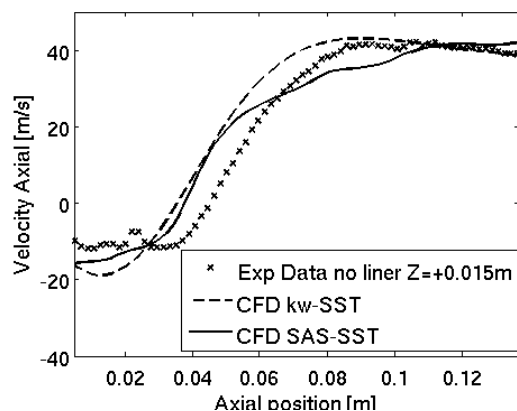


Figure 25. Axial velocity [m/s] computed on a line located at $Z=+0.015\text{m}$ for steady state and transient CFD-simulations compared to the experimental data

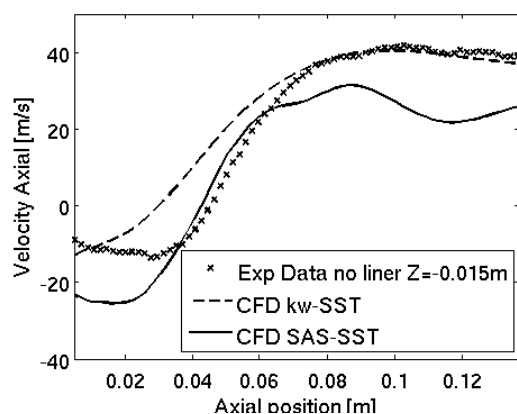


Figure 26. Axial velocity [m/s] computed on a line located at $Z=-0.015\text{m}$ for steady state and transient CFD-simulations compared to the experimental data

Figure 27 and Figure 28 show mean velocity vector field from the PIV measurements and transient averaged CFD. The SAS-SST model predicts the size of the recirculation zone well, but the magnitude of the highest velocity is not well predicted.

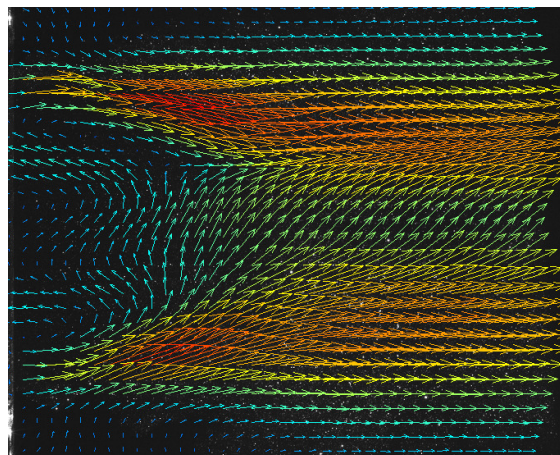


Figure 27. Mean velocity vector field from the experimental measurements, without a liner, where the range is from 0m/s (blue color) to 61m/s (red color)

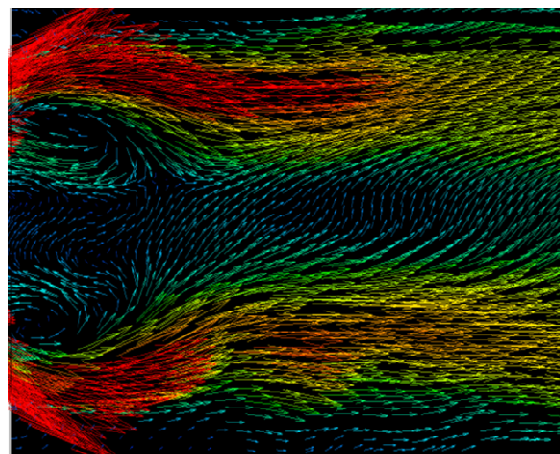


Figure 28. Mean velocity vector field from averaged transient CFD simulation (SAS-SST model) without a liner, where the range is from 0m/s (blue color) to 61m/s (red color)

CONCLUSIONS

An optimized 3-step global reaction mechanism for methane-air mixtures has been evaluated and validated in CFD analyses. A test rig burner, with three different configurations, has been modeled with the optimized 3-step global reaction mechanism using CFD.

The results from the circular liner show that the emission data (CO and O_2) are well predicted with the CFD simulations. The results from the second case with the square liner show that the velocity field and

the flame position are well predicted with the SAS-SST model, while the steady-state RANS fails in some regions. The velocity field in the open liner (unconfined flame) is not well captured by the CFD simulations.

Acknowledgments

This research has been funded by the Swedish Energy Agency, Siemens Industrial Turbomachinery AB, Volvo Aero Corporation, and the Royal Institute of Technology through the Swedish research program TURBOPOWER, the support of which is gratefully acknowledged.

Also, the computations were performed on C3SE computing resources. Thomas Svedberg at C3SE is acknowledged for assistance concerning technical aspects and implementation in making the Ansys CFX code run on the C3SE resources.

References

- [1] A. Abou-Taouk and L.E Eriksson, 2011, "Optimized Global Mechanisms For CFD Analysis Of Swirl-Stabilized Syngas Burner For Gas Turbines", ASME Turbo Power Expo, Power for land, Sea and Air, GT2011-45853.
- [2] I.R. Sigfrid, R. Whiddon, R. Collin and J.Klingmann, 2011, "Experimental Investigation of Lean Stability Limit of an Prototype Syngas Burner for Low Calorific Value Gases", ASME Turbo Power Expo, Power for land, Sea and Air, GT2011-45694.
- [3] I.R. Sigfrid, R. Whiddon, R. Collin and J.Klingmann, 2011, "Parametric Study of Emissions from Low Calorific Value Syngas Combustion, with Variation of Fuel Distribution, in a Prototype Three Sector Burner", ASME Turbo Power Expo, Power for land, Sea and Air, GT2011-45689.
- [4] Shell scenarios, <http://www.shell.com/>
- [5] Igor V. Novosselov and Philip C. Malte, 2008, "Development and application of an Eight-Step Global Mechanism for CFD and CRN Simulation of Lean-Premixed Combustors", Journal of Engineering for Gas Turbines and Power, Vol.130
- [6] P. Gokulakrishnan, S. Kwon, A.J. Hamer, M.S. Klassen and R..J. Roby, 2006, "Reduced Kinetic Mechanism for Reactive Flow Simulation of Syngas/Methane Combustion at Gas Turbine Conditions, ASME Turbo Power Expo, Power for land, Sea and Air, GT2006-90573
- [7] Karl V. Meredith and David L. Black, 2006, "Automated Global Mechanisms Generation for use in CFD Simulations", AIAA 2006-1168
- [8] D. Marlow and T.S Norton, 1995, "A Reduced Mechanism for Low-Heating-Value Gas Combustion In a Perfectly Stirred Reactor", American Flame Research Committee 1995 International Symposium
- [9] N. Slavinskaya, M. Braun-Unkhoff and P.Frank, 2008, "Reduced Reaction Mechanisms for Methane and Syngas Combustion in Gas Turbines", Journal of Engineering for Gas Turbines and Power, Vol.130'
- [10] W.P. Jones and R.P. Lindstedt, 1988, "Global Reaction Schemes for Hydrocarbon Combustion", Combustion and Flame 73: 233-249
- [11] Charles K. Westbrook and Frederick L. Dryer, 1984, "Chemical Kinetic Modeling of Hydrocarbon Combustion", Prog. Energy Combustion Sci. 1984, Vol. 10, pp. 1-57
- [12] Smith, G. P., Golden, D. M., Frenklach, M., Moriarty, N. W., Eiteneer, B., Goldenberg, M., Bowman, C. T., Hanson, R. K., Song, S., Gardiner Jr, W. C., Lissianski, V. V., and Qui, Z., 1999, "Gri-Mech 3.0,"[http://www. me. berkeley. edu/gri_mech](http://www.me.berkeley.edu/gri_mech)
- [13] <http://sourceforge.net/projects/cantera/>
- [14] B. Franzelli, E. Riber, M. Sanjose and T. Poinot, 2010, "A two-step chemical scheme for kerosene-air flames", Combustion and Flame 175:1364-1373.
- [15] Commercial software Ansys CFX, <http://www.ansys.com/default.asp>
- [16] B. F. Magnussen and B. H. Hjertager. "On mathematical models of turbulent combustion with special emphasis on soot formation and combustion". 16th Symp. (Int'l.) on Combustion. The Combustion Institute, 1976.
- [17] Menter F.R., "Two-equation eddy-viscosity turbulence models for engineering applications", AIAA-Journal., 32(8), pp. 1598 - 1605, 1994.
- [18] Egorov, Y., and Menter, F., "Development and Application of SST-SAS Turbulence Model in the DESIDER Project", Second Symposium on Hybrid RANS-LES Methods, Corfu, Greece, 2007.
- [19] Commercial software ICEM CFD, <http://www.ansys.com/default.asp>